p-(*p*,*π**) Interaction Mechanism Revealing and Accordingly Designed New Member in Deep-Ultraviolet NLO Materials $Li_nM_{n-1}B_{2n-1}O_{4n-2}$ (M=Cs/Rb, n=3, 4, 6)

Bingbing Zhang,[a,b] Zhihua Yang,[*,a] Yun Yang,[*,a] Ming-Hsien Lee,[c] Shilie Pan,[*,a] Qun Jing,[a,b] and Xin Su[a,b]

[a]Key Laboratory of Functional Materials and Devices for Special Environments of CAS; Xinjiang Key Laboratory of Electronic Information Materials and Devices; Xinjiang Technical Institute of Physics & Chemistry of CAS, 40-1 South Beijing Road, Urumqi 830011, China.
[b]University of Chinese Academy of Sciences, Beijing 100049, China;
[c]Department of Physics, Tamkang University, Taipei 25137, Taiwan
To whom correspondence should be addressed.
E-mail: zhyang@ms.xjb.ac.cn (Zhihua Yang), slpan@ms.xjb.ac.cn (Shilie Pan), yangyun@ms.xjb.ac.cn (Yun Yang)
Tel: (86)-991- 3810816
Fax: (86)-991-3838957

Electronic Supplementary Information:

Figure S1. Band structures of L3CBO, L4CBO, L6RBO, and L4RBO calculated along selected high symmetry k-points.

Figure S2. UV-Vis-IR diffuse reflectance spectrum of L3CBO, L4CBO, L6RBO, and L4RBO. Optical band gaps for L3CBO, L4CBO, L6RBO, and L4RBO are obtained by the extrapolation method.

Figure S3. The comparision between PDOS and band-resolved $\chi^{(2)}$ of (a) L3CBO, (b) L4RBO, (c) L6RBO. The energy ranges of the specific orbitals in L3CBO are marked in (d) for the further analyses.

Figure S4. Some representative orbital shapes in these six regions. Orbital N represents the N_{th} band. The eigenvalues of each orbital was marked in Figure S3d from the lowest value of the energy of the band at any k-point to the highest value of the energy of the band at any k-point.

Figure S5. The PDOS of off-ring and in-ring O atoms in L3CBO. The off-ring O atoms have more non-bonding 2*p* states than that of the in-ring O atoms.

Figure S6. The SHG-density of occupied states and unoccupied states of L6RBO in the VE process.

Figure S7. The SHG-density of occupied states and unoccupied states of L3CBO in the VE process.

Figure S8. The SHG-density of occupied states and unoccupied states of L4RBO in the VE process.

Figure S9. Coordination of oxygen atoms around Li and Rb.

Figure S10. The IR spectrum of L4RBO.

Figure S11. TG/DSC curve of L4RBO.

Figure S12. Experimental and calculated XRD patterns of L4RBO compared with the pattern after melting.

Figure S13. The charger distribution of B (green) and O (red) atoms of siolated B_7O_{14} group in L4CBO (top) and L4RBO (bottom) as well as the related dipole moment.

Table S1. Atomic coordinates and equivalent isotropic displacemnt parameters for L4RBO. U_{eq} is defined as one third of the trace of the orthogonalized U_{ij} tensor.

Table S2. Bond lengths and angles for L4RBO.

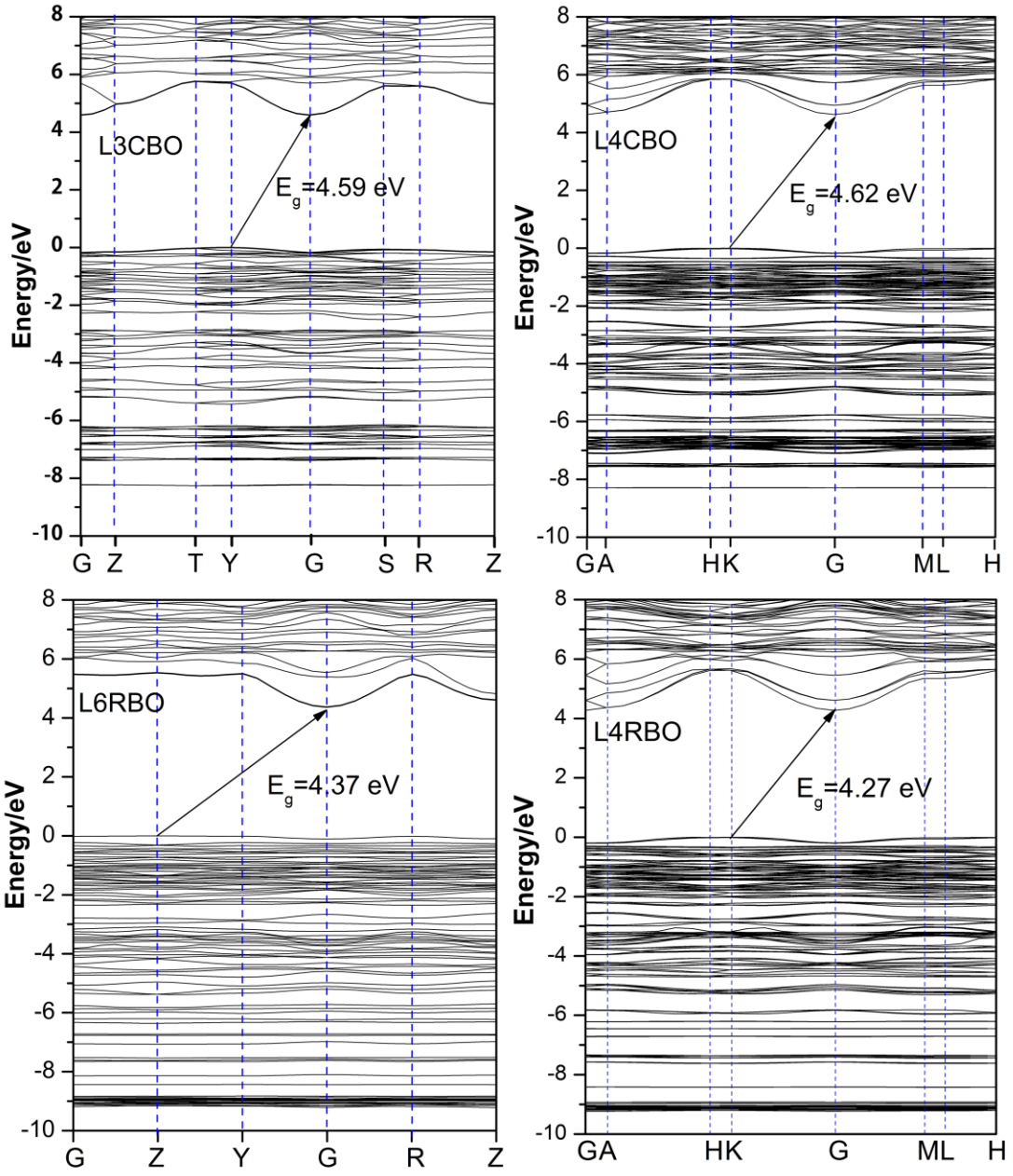

Figure S1. Band structures of L3CBO, L4CBO, L6RBO, and L4RBO calculated along selected high symmetry k-points. Their band structures are qualitatively similar to one another with indirect band gap.

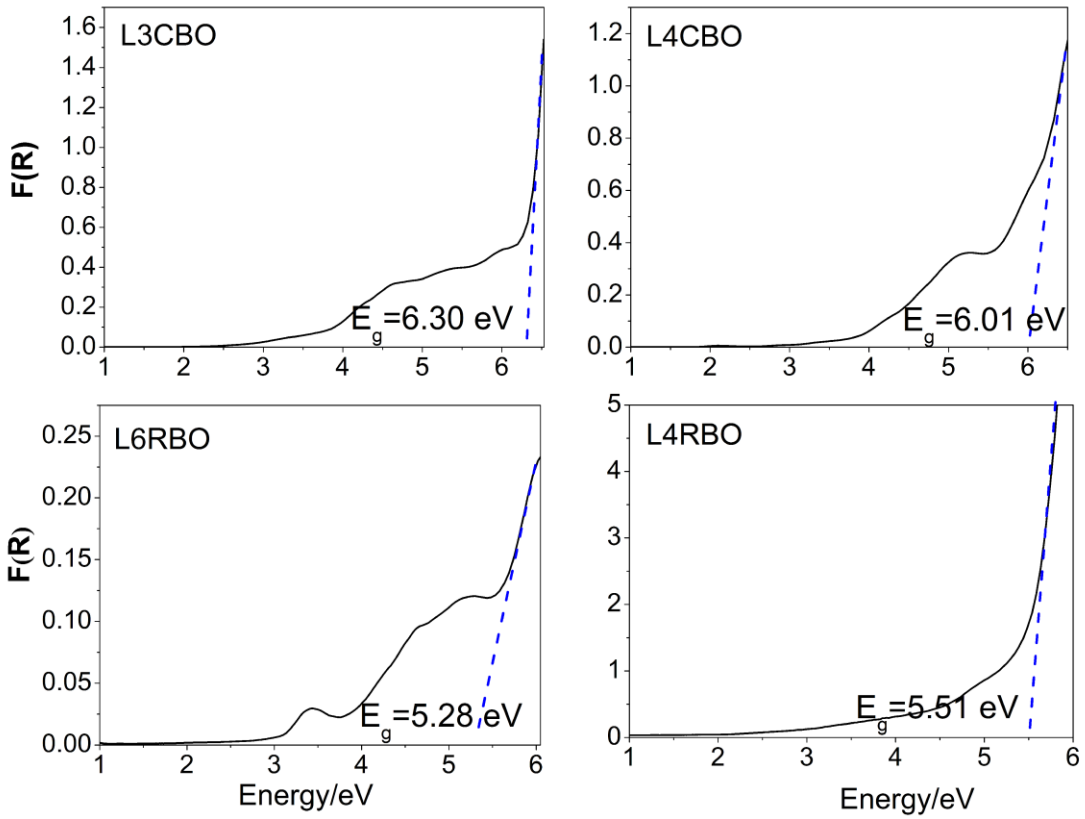

Figure S2. UV-Vis-IR diffuse reflectance spectrum of L3CBO, L4CBO, L6RBO, and L4RBO. Optical band gaps for L3CBO, L4CBO, L6RBO, and L4RBO are obtained by the extrapolation method.[1]

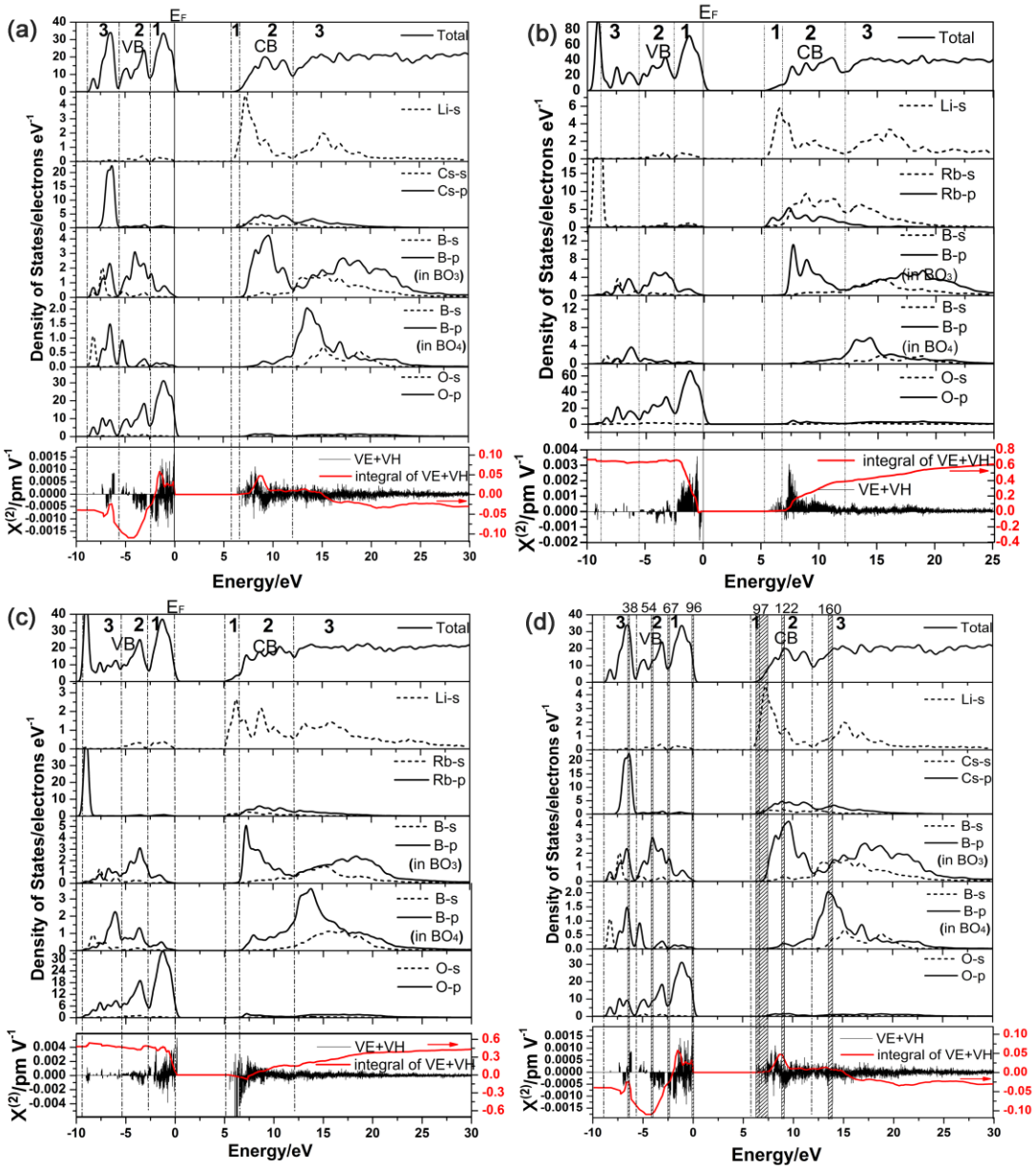

Figure S3. The comparision between PDOS and band-resolved $\chi^{(2)}$ of (a) L3CBO, (b) L4RBO, (c) L6RBO. The energy ranges of the specific orbitals in L3CBO are marked in (d) for the further analyses.

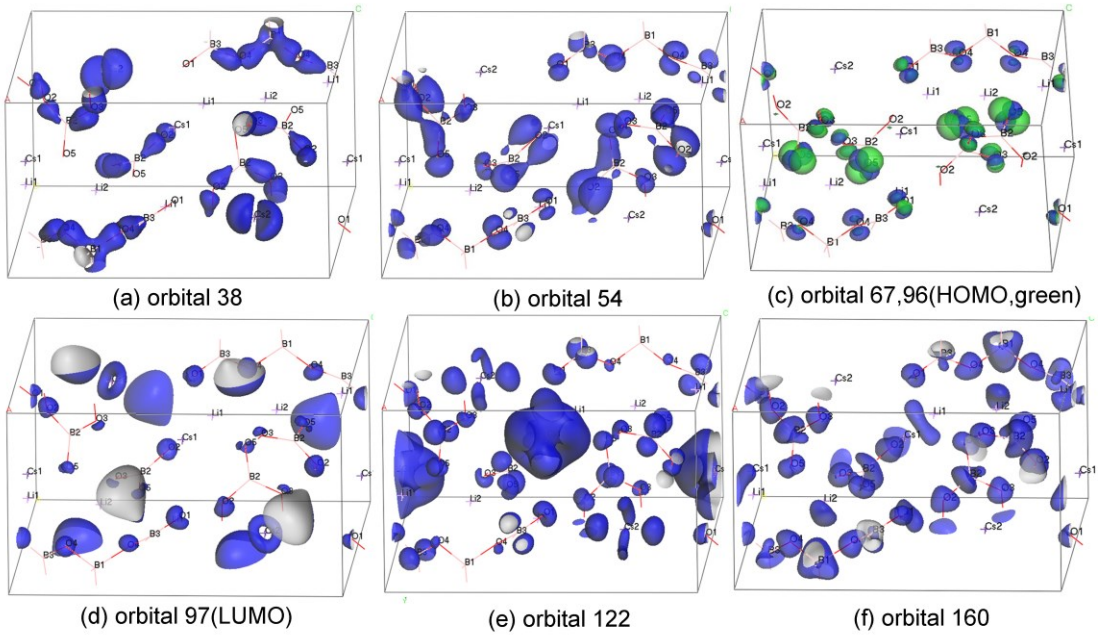

Figure S4. Some representative orbital shapes in these six regions. Orbital N represents the Nth band. The eigenvalues of each orbital was marked in Figure S3d from the lowest value of the energy of the band at any k-point (in eV) to the highest value of the energy of the band at any k-point (in eV).

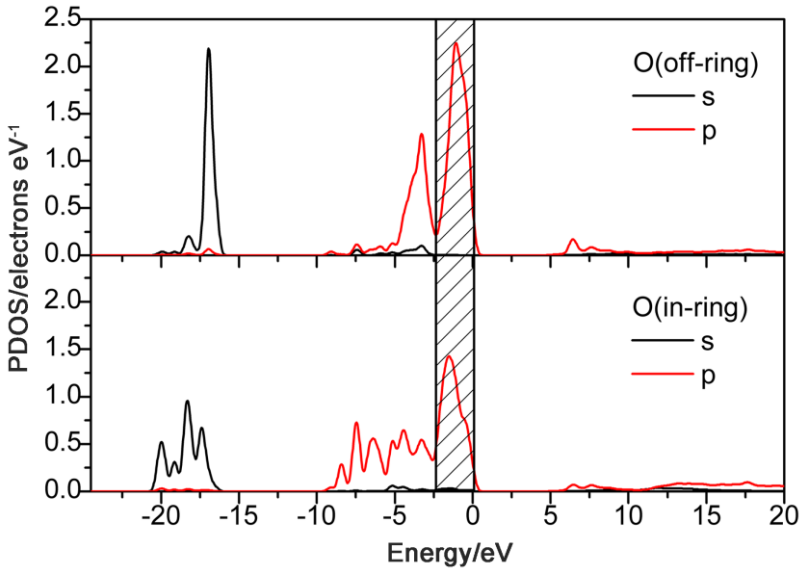

Figure S5. The PDOS of off-ring and in-ring O atoms in L3CBO. The off-ring O atoms have more non-bonding 2*p* states than that of the in-ring O atoms.

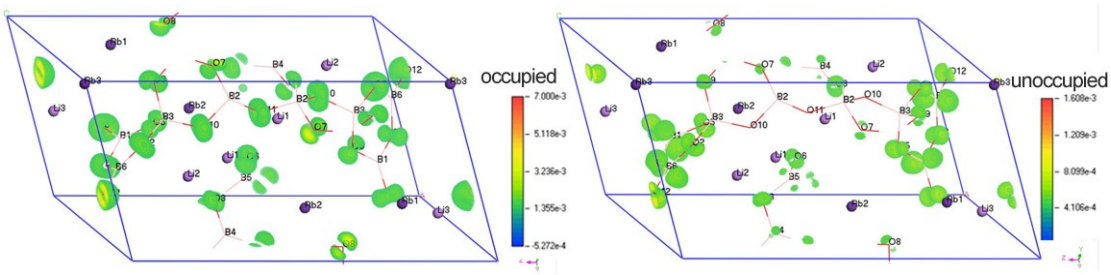

Figure S6. The SHG-density of occupied states (left) and unoccupied states (right) of L6RBO in the VE process.

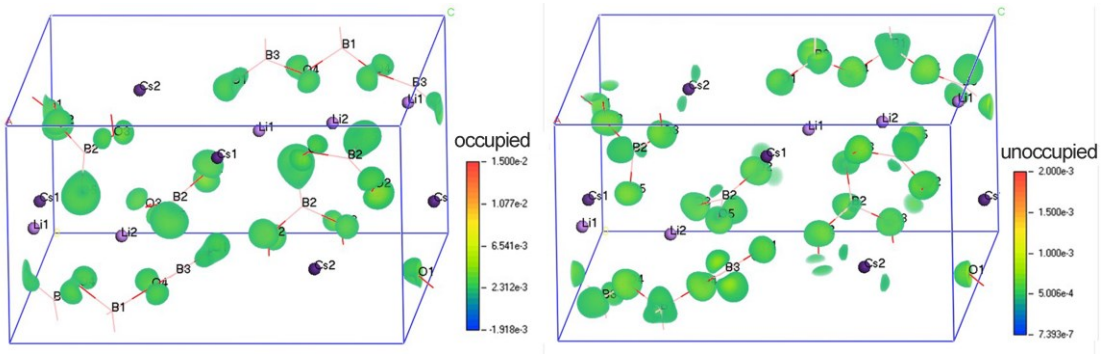

Figure S7. The SHG-density of occupied states (left) and unoccupied (right) states of L3CBO in the VE process.

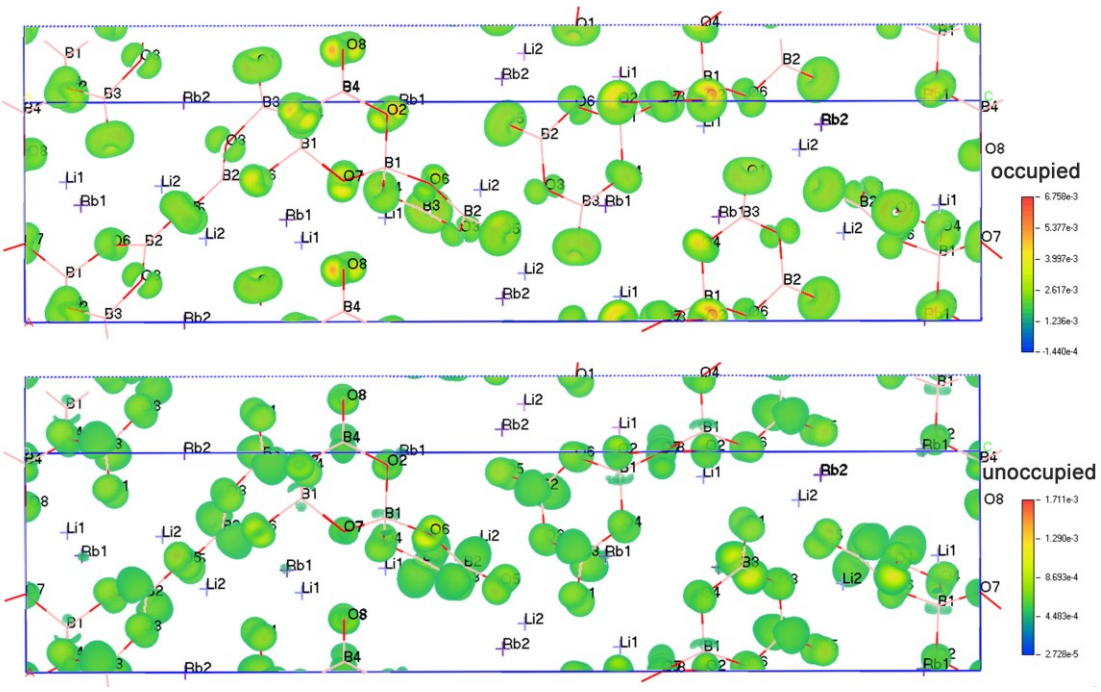

Figure S8. The SHG-density of occupied states (top) and unoccupied states (bottom) of L4RBO in the VE process.

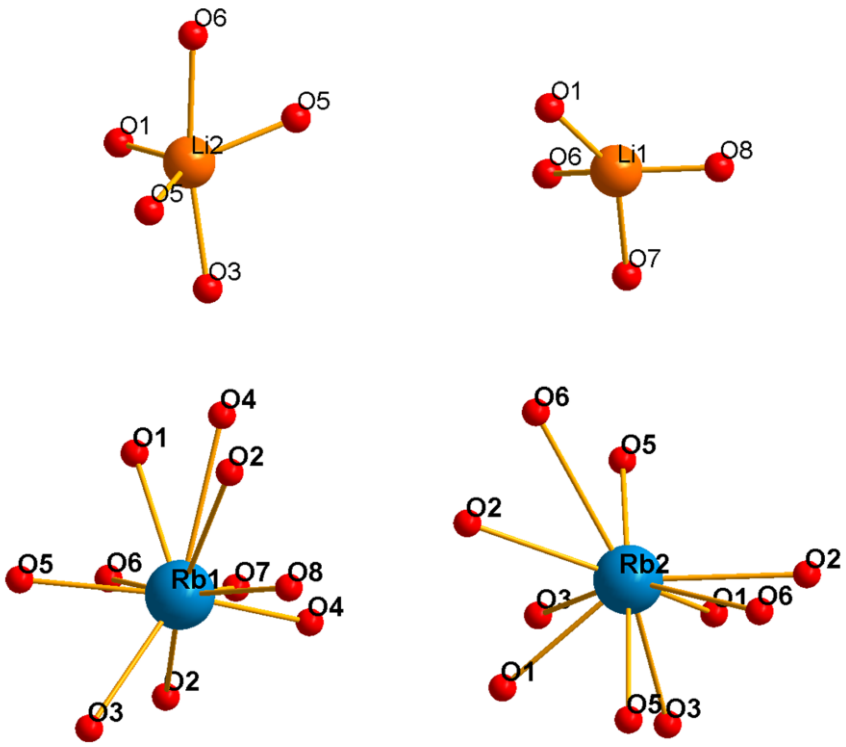

Figure S9. Coordination of oxygen atoms around Li and Rb.

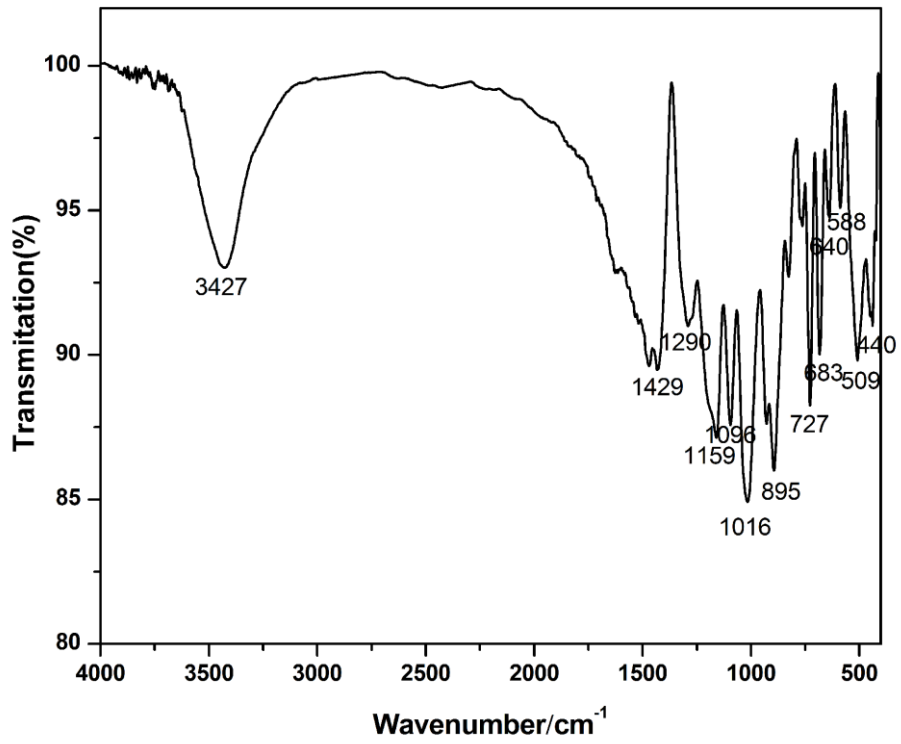

Figure S10. The IR spectrum of L4RBO.

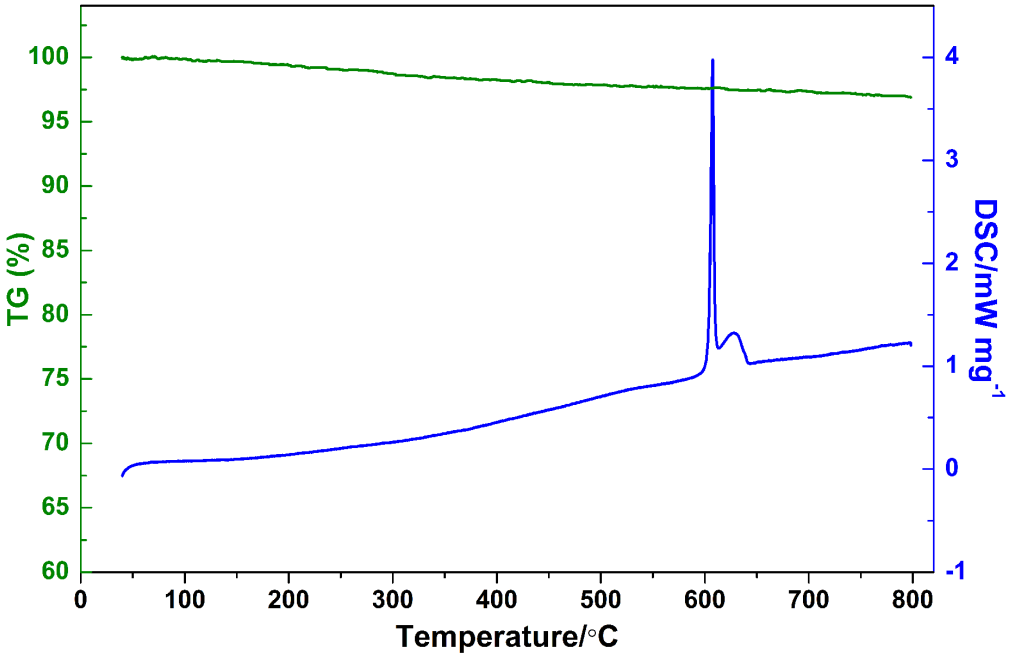

Figure S11. TG/DSC curve of $Li_4Rb_3B_7O_{14}$.

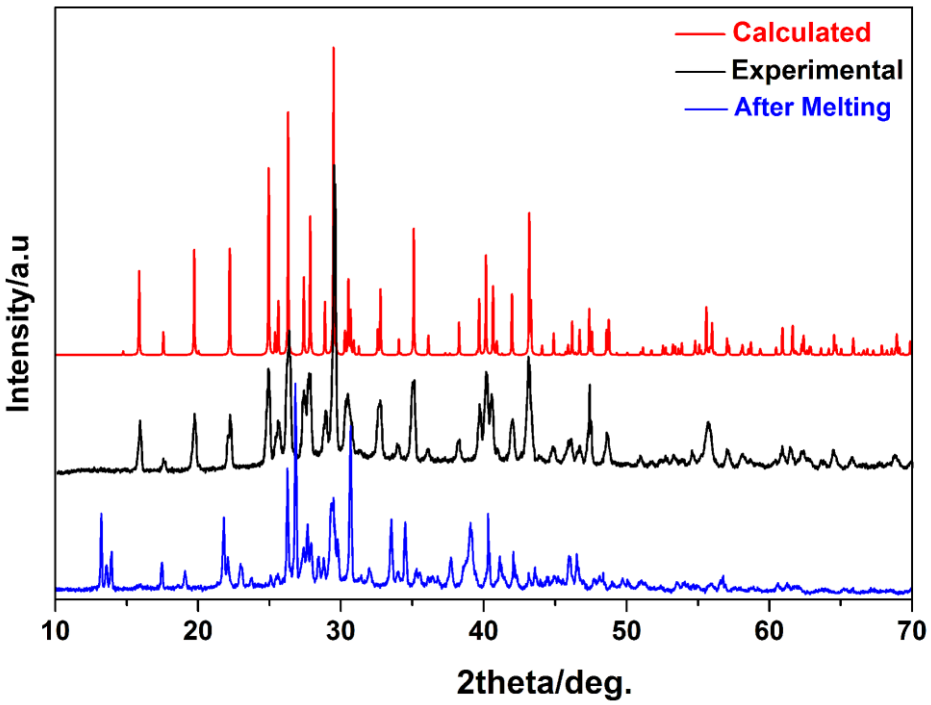

Figure S12. Experimental and calculated XRD patterns of L4RBO compared with the pattern after melting.

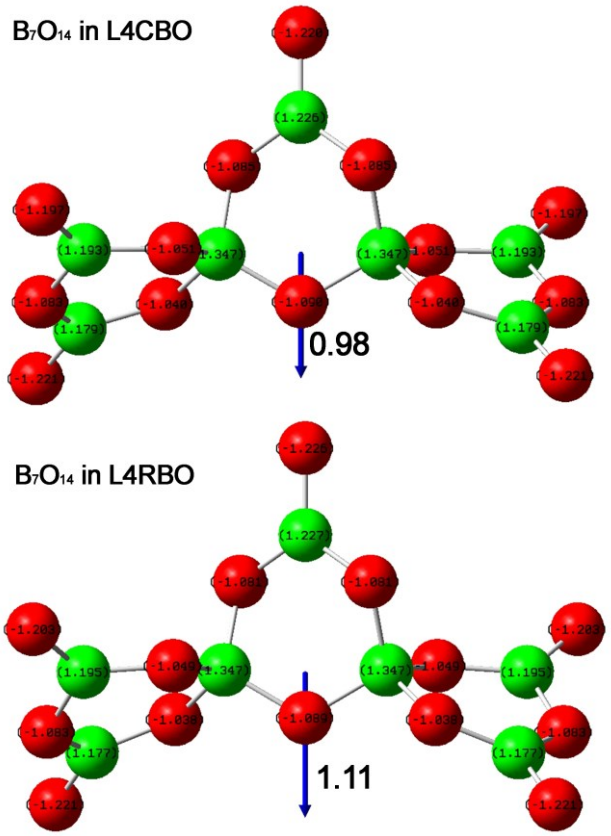

Figure S13. The charger distribution of B (green) and O (red) atoms of siolated B_7O_{14} group in L4CBO (top) and L4RBO (bottom) as well as the related dipole moment.

Table S1. Atomic coordinates ($\times 10^4$) and equivalent isotropic displacemnt parameters ($Å^2 \times 10^3$) for $Li_4Rb_3B_7O_{14}$. U_{eq} is defined as one third of the trace of the orthogonalized U_{ij} tensor.

Atom	x	y	z	U_{eq}
Rb(1)	4658(1)	9910(1)	594(1)	20(1)
Rb(2)	0	11058(1)	1667	20(1)
Li(1)	3616(8)	14739(8)	439(2)	14(1)
Li(2)	3803(9)	6001(8)	1437(2)	14(1)
B(1)	7937(6)	7017(6)	436(1)	10(1)
B(2)	6478(5)	14799(5)	1264(1)	8(1)
B(3)	-198(6)	5062(6)	836(1)	9(1)
B(4)	478(8)	10478(8)	0	18(1)
O(1)	1703(3)	5066(3)	895(1)	11(1)
O(2)	-530(3)	9418(3)	460(1)	18(1)
O(3)	8081(3)	14114(3)	1223(1)	11(1)
O(4)	5877(4)	9265(4)	-408(1)	20(1)
O(5)	4968(4)	14001(3)	1640(1)	11(1)
O(6)	6480(3)	6275(3)	903(1)	10(1)
O(7)	6413(4)	6413(4)	0	9(1)
O(8)	2414(5)	12414(5)	0	34(1)

Table S2. Bond lengths [Å] and angles [deg] for $Li_4Rb_3B_7O_{14}$.

Rb(1)-O(4)	2.8304(19)	B(2)-Li(2)#6	2.406(6)
Rb(1)-O(5)#1	2.9524(19)	B(3)-O(1)	1.315(4)
Rb(2)-O(5)	2.976(2)	B(3)-O(4)#3	1.373(3)
Li(1)-O(8)	1.793(5)	B(3)-O(3)#12	1.435(4)
Li(1)-O(1)#6	1.863(5)	B(4)-O(8)	1.331(6)
Li(1)-O(7)#6	2.027(5)	B(4)-O(2)#9	1.389(3)
Li(1)-O(6)#6	2.088(5)	B(4)-O(2)	1.389(3)
Li(1)-B(1)#6	2.574(6)	O(1)-Li(1)#2	1.863(5)
Li(1)-Li(1)#9	2.641(9)	O(2)-B(1)#8	1.450(4)
Li(1)-Li(2)#6	2.711(6)	O(3)-B(3)#13	1.435(4)
Li(2)-Li(1)#2	2.711(6)	O(6)-Li(1)#2	2.088(5)
B(1)-O(2)#10	1.450(4)	O(7)-B(1)#11	1.454(3)
B(1)-O(7)	1.454(3)	O(7)-Li(1)#3	2.027(5)
B(1)-O(4)#11	1.473(4)	O(7)-Li(1)#2	2.027(5)
B(1)-O(6)	1.489(3)	O(8)-Li(1)#9	1.793(5)
B(1)-Li(1)#2	2.574(6)	B(2)-O(3)	1.403(3)
B(2)-O(5)	1.326(4)	B(2)-Li(2)#7	2.361(6)
B(2)-O(6)#6	1.380(4)		
O(4)-Rb(1)-O(5)#1	142.30(6)	Li(1)#2-Rb(1)-B(3)	51.97(10)
O(3)-Rb(1)-O(8)	95.47(6)	Li(2)-Rb(1)-B(3)	52.21(10)
O(4)-Rb(1)-Li(1)#2	68.89(9)	O(4)#3-Rb(1)-B(3)	23.40(6)
O(3)-Rb(1)-Li(2)	98.85(9)	O(4)-Rb(1)-O(6)	81.63(5)
O(8)-Rb(1)-Li(2)	144.95(10)	O(1)-Rb(1)-B(2)	131.99(6)
O(8)-Rb(1)-B(3)	96.56(8)	O(1)#5-Rb(2)-O(3)#7	44.44(5)
O(5)-Rb(2)-B(3)#5	84.08(7)	O(1)#6-Rb(2)-O(3)#7	60.98(5)
O(5)#4-Rb(2)-B(3)#5	86.24(7)	O(3)#8-Rb(2)-O(2)#4	128.69(5)
B(3)#5-Rb(2)-B(3)#6	74.80(10)	O(5)-Rb(2)-O(2)	95.95(5)
O(7)#6-Li(1)-O(6)#6	69.43(17)		

1. Schevciw, O.; White, W. B., *Mater. Res. Bull.* **1983,** *18* (9), 1059-1068.